Control of the Chemical Step by Leucine-31 of Pancreatic Phospholipase A_2[†]

Bao-Zhu Yu,[‡] Marcel J. W. Janssen,[§] Hubertus M. Verheij,[§,||] and Mahendra Kumar Jain*,[‡]

Department of Chemistry and Biochemistry, University of Delaware, Newark, Delaware 19716, and Department of Enzymology and Protein Engineering (CBLE, Institute of Biomembranes), Faculty of Chemistry, Utrecht University, Utrecht, The Netherlands

Received November 4, 1999; Revised Manuscript Received February 7, 2000

ABSTRACT: A well-defined region of pancreatic and other secreted phospholipase A_2 (PLA2), which we call the i-face, makes a molecular contact with the interface to facilitate and control the events and processivity of the interfacial catalytic turnover cycles. The structural features of the i-face and its allosteric relationship to the active site remain to be identified. As a part of the calcium binding (26−34) loop, Leu-31 is located on the surface near the substrate binding slot of PLA2. Analysis of the primary rate and equilibrium parameters of the Leu-31 substitution mutants of the pig pancreatic PLA2 shows that the only significant effect of the substitution is to impair the chemical step at the zwitterionic interface in the presence of added NaCl, and only a modest effect is seen on k^*_{cat} at the anionic interface. Leu-31 substitutions have little effect on the binding of the enzyme to the interface; the affinity for certain substrate mimics is modestly influenced in W3F,L31W double mutant. The fluorescence emission results with the double mutant show that the microenvironment of Trp-31 is qualitatively different at the zwitterionic versus anionic interfaces. At both of the interfaces Trp-31 is not shielded from the bulk aqueous environment as it remains readily accessible to acrylamide and water. The NaCl-induced change in the Trp-31 emission spectrum of the double mutant on the zwitterionic interface is similar to that seen on the binding to the anionic interface. Together, the kinetic and spectroscopic results show that the form of PLA2 at the zwitterionic interface (E_z*) is distinguishably different from the catalytically more efficient form at the anionic interface (E_a*). This finding provides a structural basis for the two-state model for k^*_{cat} activation by the anionic interface. In conjunction with earlier results we suggest that neutralization of certain cationic residues of PLA2 exerts a control on the calcium loop through residue 31.

A functional relationship between the catalytic and the interfacial binding events is the hallmark of interfacial enzymology within the following kinetic paradigm (*1*−*7*):

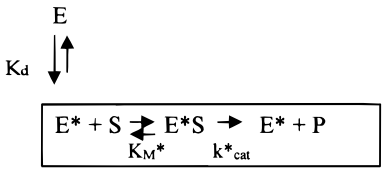

The effective turnover of interfacial enzymes is determined by relationships between the binding of the enzyme to the interface (E to E*) and other interfacial exchange processes implicit in this scheme, including the exchange of the substrate and product. Such events collectively determine the microscopic steady-state condition for the catalytic cycle (boxed) by controlling the "local" concentrations that determine the fraction of the enzyme at the interface (E*) and what the bound enzyme "sees".

In our quest to develop an analytical basis for interfacial enzymology, with secreted phospholipase A_2 (PLA2)[1] as the prototype, we have established methods to obtain the primary interfacial binding and catalytic parameters, including K_d, K_M*, and k^*_{cat} (*1*−*14*). Such a detailed kinetic analysis is possible only under the scooting (*1*−*5*) or the quasi-scooting (*6*, *7*) modes. With a highly processive turnover at the interface, the microscopic steady-state condition can be unequivocally defined as the enzyme binding and desorption steps of the E to E* equilibrium are not a part of the catalytic turnover cycle. The incremental changes in the primary parameters, for each of the steps in the kinetic scheme above, associated with the residue substitutions are useful for discerning the functional role of specific structural features of PLA2. Thus it is possible to discern the observed kinetic effect of a residue substitution in terms of the change in the

[†] This work was supported by the USPHS (Grant GM29703 to M.K.J.).

* To whom correspondence should be addressed: e-mail mkjain@udel.edu; phone 302-831-2968; fax 302-831-6335.

[‡] University of Delaware.

[§] Utrecht University.

[||] Professor H. M. Verheij passed away in a tragic accident on Aug 1, 1998.

[1] Abbreviations: cmc, critical micelle concentration; DC_nPC, 1,2-diacylglycero-*sn*-3-phosphocholine (n = 6−8); DC_8PM, 1,2-dioctanoylglycero-*sn*-3-phosphomethanol; deoxy-LPC, 1-hexadecylpropanediol-3-phosphocholine; DMPM, 1,2-dimyristoylglycero-*sn*-3-phosphomethanol; DTPM, 1,2-ditetradecylglycero-*sn*-3-phosphomethanol; HPM, hexadecylphosphomethanol; L, an active site directed mimic such as a substrate, product, or competitive inhibitor; MF, mole fraction unit; MJ33, 1-hexadecyl-3-(trifluoroethyl)-*rac*-glycero-2-phosphomethanol; PC8-ether, 1,2-dioctylphosphatidylcholine; PLA2, phospholipase A_2 from pig pancreas unless noted otherwise; PN, hexadecyl-1-phosphocholine. The i-face of an interfacial enzyme makes contact with the substrate interface. Analytical relationships for the rate and equilibrium constants are developed elsewhere (*3*, *5*−*7*).

10.1021/bi9925470 CCC: $19.00
Published on Web 04/18/2000

binding of the enzyme to the interface, or the substrate binding to the active site, or on the chemical step, or on the allosteric modulation of the catalytic cycle events (*9*−*14*).

In this paper we analyze the effects of Leu-31 substitution in pig pancreatic PLA2. On the basis of the crystallographic (*14*−*16*) and NMR structures (*17*−*19*), the biochemical, spectroscopic, and kinetic results (*3*, *12*, *13*, *20*, *21*) have provided a consensus His-48/Asp-99 diad with a calcium cofactor for the catalytic cycle (*12*, *20*, *21*). Leu-31 is a part of the EF motif of the (26−34) loop in which the backbone carbonyls of the highly conserved residues Tyr-28, Gly-30, and Gly-32 provide three oxygen ligands for the calcium binding. While calcium does not have an effect on the binding of the enzyme to the interface, it is an obligatory cofactor for the substrate binding and for the rate-limiting chemical step (*12*). The calcium loop is flexible in the solution NMR structure (*17*), which raises the possibility that the loop could be influenced by the interface as an allosteric modulator for the interfacial catalytic turnover steps. The functional significance of Leu-31 is also implicated by its localization at the putative entrance to the active site slot (*16*, *21*−*23*). Leu-31 is not conserved in the evolutionarily divergent secreted PLA2; it is often replaced by Ala, Pro, Lys, Arg, or Trp (*21*). However, the possibility of a direct hydrophobic contact of residue 31 with the interface has been raised (*14*, *16*, *24*, *25*).

A detailed kinetic analysis of the Leu-31 substitution mutants as developed in this paper shows that the substitutions significantly lower the k^*_{cat} at the zwitterionic interface, whereas only a modest effect is seen for the turnover at the anionic interface. The kinetic and spectroscopic results show that the enzyme at the interface exists in two distinct forms, E_a^* at the anionic interface and E_z^* at the zwitterionic interface. This provides a basis for k^*_{cat} activation by the interfacial anionic charge (*6*, *9*) with the assumption that the catalytic efficiency of the Michaelis complex at the anionic interface is significantly more pronounced.

EXPERIMENTAL PROCEDURES

All experimental conditions and analytical protocols for this study have been established before (*1*−*14*, *24*), and only salient details are given in the text and figure captions. DC_nPC and PC8-ether were from Avanti Polar Lipids. PN, MJ33, DC_8PM, HPM, DTPM, and DMPM (*1*, *26*) were synthesized. All commercially available reagents were of analytical grade. Construction and preliminary kinetic characterization of the Leu-31 substitution mutants (nos. 1−9 in Table 1) have been described along with the kinetic results in Table 1 (*24*, *25*, *29*−*37*).

The steady-state fluorescence emission properties were monitored on an SLM AB2 spectrofluorometer equipped with software for data acquisition and processing. The steady-state fluorescence emission measurements are primarily intended to provide information about the changes in the microenvironment of Trp-31 in the W3F,L31W double mutant under kinetically relevant conditions. Note that the pig pancreatic PLA2 contains only one tryptophan residue. The protocols to monitor the fluorescence properties of Trp-3 in WT (*2*, *27*, *28*) were used for the characterization of the fluorescence properties of the W3F,L31W double mutant. All fluorescence measurements were carried out under identical conditions except as noted in the figure legends. Typically, a 1.55 mL solution of the 1.0 μM W3F,L31W mutant protein in 10 mM Tris buffer at pH 8.0 (or at measured pH 7.6 in the 98% D_2O buffer) and the specified additives were used in stirred cuvettes with excitation at 280 nm and 4 nm slit widths. The background spectrum (dark current and Raman scattering) was subtracted, and the correction for the lamp intensity was not made. The fluorescence emission spectra and the difference spectra are presented on a common relative scale with the peak intensity normalized to 1.0 for the E form of the 1 μM W3F,L31W mutant without calcium in the aqueous phase.

Experimental protocols for the analysis of processive turnover in the scooting mode on DMPM vesicles (*1*, *3*), or the hydrolysis of DC_7PC micelles under the quasi-scooting mode with rapid substrate replenishment, were as described before (*6*). Typically, kinetic measurements were carried out in 1 mM $CaCl_2$ and 1 mM NaCl at 25 °C and pH 8.0 under a stream of nitrogen by the pH-stat method using a Brinkman (Metrohm) or a Radiometer titrator with 3 mM NaOH titrant. Typically the reaction was initiated by the addition of 0.1−30 pmol of PLA2 in 1−30 μL volume. The water-soluble inhibitor MJ33, if present, was added during or before the reaction progress. Titration efficiency under specified conditions was determined by adding a known amount of myristic

Table 1: Apparent Rate Parameters for the Hydrolysis of Micellar DC_8PC and of Monodisperse Dithio-DC_6PC by Pig Pancreatic PLA2 Mutants

no.	mutant (ref)	V_M^{app} (DC_8PC) (μmol mg^{-1} min^{-1})	$(k_{cat}/K_m)^{app}$ (dithio-DC_6PC)
1	WT (*24*)	2200	890
2	W3F (*25*)	330	830
3	L31A (*24*)	60	160
4	L31G (*24*)	40	70
5	L31R (*24*)	180	380
6	L31S (*24*)	50	160
7	L31T (*24*)	50	110
8	L31W (*24*)	600	2450
9	W3F,L31W (*25*)	320	1590
10	M8,20L,9R (*29*)	1320	180
11	−R53K (*29*)	1710	250
12	−R53Q (*29*)	3160	380
13	−R53E (*29*)	4470	1310
14	−108K (*30*)	1500	150
15	−56K (*30*)	1180	250
16	−56Q (*30*)	4800	670
17	−56K−C2 (*30*)	2605	570
18	−56K−C8 (*30*)	4524	500
19	−108K−C14 (*30*)	2195	200
20	D66N (*31*)	2074	1172
21	Y69F (*32*)	440	1300
22	Y69K (*32*)	230	1350
23	E71N (*31*)	5043	1300
24	E92Q (*31*)	1742	890
25	N117W (*33*)	1570	800
26	N117W,D119Y (*33*)	1380	700
27	K116Y, N117W,D119Y (*33*)	550	290
28	Δ(62−66) (*34*)	5260	1790
29	−52F (*24*)	4750	1605
30	−69F (*35*)	955	7930
31	−69F,53M (*35*)	906	9051
32	−69F,56M (*35*)	1733	57958
33	−69F,53M,56M (*35*)	1730	19107
34	−73F (*24*)	4360	1310
35	−D99N (*24*)	172	1070
36	Δ(62−66),M8,20L (*36*)	6000	1400
37	−T47M (*37*)	5603	1431

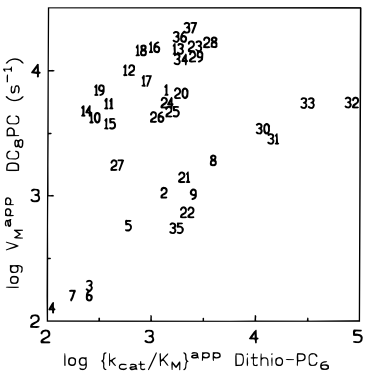

FIGURE 1: Comparison (on the log−log scale) of the apparent rate parameters (Table 1) for the hydrolysis of monodisperse dithio-PC6 (*x*-axis) and DC_8PC by the site-directed mutants of pig pancreatic PLA2. The numbers in the figure refer to the mutant numbers in Table 1.

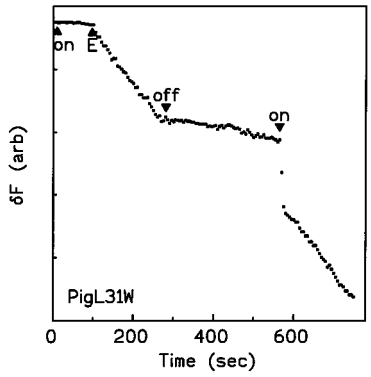

FIGURE 2: Reaction progress curve for the hydrolysis of 0.44 mM DC_6PC by 14.1 μg of the L31W mutant of PLA2 in a 2 mL reaction mixture in a plastic fluorescence cuvette under conditions described elsewhere (*38*). The reaction progress is monitored as a change in the fluorescence emission from a pH indicator dye SNAFL for which a decrease in pH lowers the fluorescence emission intensity. The reaction is initiated by adding the enzyme to the stirred reaction mixture. The stirrer is turned on and off as indicated. The rate of hydrolysis in the stirred solution is 0.11 s^{-1}.

acid or heptanoic acid to the reaction mixture in the absence of PLA2. The reaction progress for the hydrolysis of monodisperse DC_6PC without spurious kinetic contributions from the cuvette walls was monitored as established before (*38*). The rate parameters are expressed as turnover number per second. Uncertainty in the measured parameters is 10%, and parameters derived from curve fitting have up to 30% standard deviation.

Protocols for determining the primary interfacial kinetic parameters have been described before (*3*, *5*, *6*). K_M* and υ_o from the reaction progress for the hydrolysis of DMPM were determined under the polymyxin-mediated substrate replenishment conditions *(3*, *5*). Hydrolysis of DC_7PC micelles is characterized as K_M^{app} and V_M^{app} (*6*) obtained from the hyperbolic dependence of the rate of hydrolysis on the concentration of micellar DC_7PC, i.e., the total concentration minus the cmc (=1.5 mM cmc at 0.1 M NaCl or 0.1 mM cmc at 4 M NaCl).

RESULTS

Apparent Rate Parameters of the Pig Pancreatic Mutants. Two sets of apparent rate parameters for 37 pig PLA2 mutants reported from the Utrecht laboratory are summarized in Table 1. Both of the parameters for a given mutant were determined by the same experimenter, which minimizes the possibility of systematic errors in the two rates. The apparent first-order rate constant $(k_{cat}/K_m)^{app}$ is for the hydrolysis of monodisperse 1,2-dihexanoyl-1,2-dithioglycerophosphocholine (dithio-PC6). In Figure 1 it is plotted on the log−log scale against V_M^{app} for the same mutant obtained at the bulk saturating concentrations of DC_8PC micelles. Two sets of rate parameters appear to correlate with each other,; that is, each of the substitutions changes both of the activities in the same direction. However, two clusters are apparent in Figure 1. The upper cluster includes WT (no. 1), and the mutants in the lower cluster have significantly lower V_M^{app} with a wider range for $(k_{cat}/K_m)^{app}$. It is striking that the lower cluster has all of the Leu-31 (nos. 3−9), Asp-99 (no. 35), and Tyr-69 (nos. 21, 22, 30−33) substitution mutants. This correlation suggests that these three residues play a role that is not analogous to any other substitution in Table 1.

In the consensus catalytic mechanism for PLA2 (*12*), Tyr-69 and Asp-99 play a role in the events of the catalytic cycle at the interface (*12*, *16*, *20*). Also, Asp-99 (*13*) and Tyr-69 (*12*) substitutions impair k^*_{cat} of pancreatic PLA2 at the zwitterionic and anionic interfaces without a significant effect on the binding of the enzyme to the interface, as well as on the mimic binding to the E* form. On the basis of the results in Figure 1, the implication is that Leu-31 also plays a role in controlling the turnover on DC_8PC micelles. This is a significant and surprising result because Leu-31 has not been implicated directly in a catalytic mechanism. A role for Leu-31 in the binding of PLA2 to the interface has been suggested (*16*), and also an enhanced catalytic efficiency of type V PLA2, relative to type IIa, has been attributed to the effect of Trp-31 on the binding of type V PLA2 to the interface (*38*). In any case, such effects cannot account for lower V_m^{app} for the Leu-31 mutant.

Monomer Rate. The $(k_{cat}/K_m)^{app}$ parameter in Table 1 and Figure 1 is believed to be for the hydrolysis through the monodisperse Michaelis complex. Elsewhere, we have shown that such rates are largely an artifact of the reaction at extraneous surfaces such as the cuvette walls (*39*), and this is the case with the Leu-31 mutants. For example, as shown in Figure 2, contributions of extraneous surfaces to the observed rate can be readily eliminated. In this assay the release of the fatty acid product is monitored as the fluorescence change reported by a pH indicator. In the stirred reaction mixture the reaction progress starts soon after the addition of the L31W (no. 8) mutant; however, the fluorescence change ceases as soon as the stirring is turned off. On the basis of such measurements, our limit estimate for the rate of hydrolysis of monodisperse DC_6PC by WT or the Leu-31 mutants is significantly below 0.1 s^{-1}. These upper limit estimates are considerably smaller than the "monomer rates" in Table 1, which are typically in the range of the rates seen in stirred cuvettes. We conclude that the monomer rates in Table 1 are due to the reaction on the walls of the plastic cuvette used for the monomer assays.

Parameters for the Processive Kinetics of Leu-31 Substitution Mutants. Several parameters for the Leu-31 substitution mutants are summarized in Table 2. They relate to the individual steps of the interfacial catalytic turnover cycle at the anionic bilayer (DMPM) and zwitterionic micellar

Table 2: Equilibrium Binding and Kinetic Parameters for Pig Pancreatic PLA2 Mutants

			DMPM				DC_7PC 1 mM NaCl		DC_7PC 4 mM NaCl		
no.	enzyme	K_{Ca}* (mM)	K_{Ca}*(S) (mM)	K_M* (MF)[a]	v_o (s^{-1})	X_I(50) (MF)	V_M^{app} [b]	K_M^{app} [c]	V_M^{app} [b]	K_M^{app} [c]	X_I(50)
1	WT	0.25	0.09	0.35	300	0.006	16	2.3	660	0.2	0.012
2	W3F	0.13			160	0.011	2	3.0	78	0.15	0.013
3	L31A	0.45	0.17	0.6	230	0.014	1		27	0.1	0.04
4	L31G	1.4	0.2	0.2	175	0.022	2		20	0.1	0.02
5	L31R	0.77	0.18	0.3	125	0.008	1		20	0.1	0.02
6	L31S	0.43	0.18	0.7	154	0.012	1	1.8	16	0.34	0.03
7	L31T	0.25	0.11	0.9	125	0.02	2		13	0.21	0.04
8	L31W	0.1	0.13	0.5	105	0.022	4	2.8	60	0.13	0.008
9	W3F,L31W	0.6	0.08	0.1	140	0.0005	7	3.4	21	0.18	0.02

[a] MF = mole fraction. [b] Units are s^{-1}. [c] Units are mM.

(DC_7PC) interfaces and are directly relevant for evaluating the origin of the changes in V_M^{app} for DC_8PC (Table 1). The dissociation constant for the E*·Ca complex on the interface of deoxy-LPC, the K_{Ca}* values in column 3 of Table 2, are in a 10-fold range. Larger K_{Ca}* values relative to WT suggest an unfavorable change in the calcium binding loop of the E* form at the zwitterionic interface of deoxy-LPC, a neutral diluent with little affinity for the active site of WT (*26*, *40*). A marginally lower K_{Ca}* for the L31W (no. 8) or W3F (no. 2) implies an intrinsically higher affinity for calcium. However, it may also be an apparent value due to the calcium-dependent binding of deoxy-LPC to the active site (see below) because it cannot be assumed a priori that deoxy-LPC would not bind to the active site of a mutant. To ensure that deoxy-LPC does not bind to the active site of the mutant, one would require another neutral diluent, which we do not have. However, on the basis of the magnitude of the K_{Ca}* values, we believe that the calcium-dependent dissociation constant for the binding of deoxy-LPC is not smaller than 0.5 mole fraction for L31T, compared to a value of more than 2 mole fractions for WT (see below).

K_{Ca}*(S), column 4 of Table 2, is the apparent kinetic dissociation constant for calcium from E*·Ca·S, the ternary Michaelis complex, formed during the processive catalytic turnover on DMPM vesicles at $X_S = 1$. Since the substrate binding obligatorily requires calcium (*40*), K_{Ca}*(S) is an apparent value for the two-step sequential equilibrium:

$$E^* + Ca \overset{K_{Ca}^*}{\rightleftharpoons} E^*\cdot Ca + S \overset{K_M^*}{\rightleftharpoons} E^*\cdot Ca\cdot S \rightarrow \text{hydrolysis}$$

$$K_{Ca}^*(S) = \frac{K_{Ca}^*}{1 + 1/K_M^*} \quad (1)$$

It holds for the formation of the ternary E*·Ca·L complexes of all active site directed mimics (*12*, *40*). As expected from eq 1, K_{Ca}* is significantly larger than K_{Ca}*(S) for all mutants except L31W. Note that K_{Ca}*(S) values for all the mutants in Table 2 are in a 2.5-fold range, which suggests a modest change in the stability of the E*·Ca·DMPM ternary complex. The K_M* values for DMPM (column 5), calculated from the two calcium binding parameters (eq 1), are in a range of 0.1−0.9 mole fraction. Considering a 30% uncertainty in the value of each of the component calcium binding parameters, we conclude that K_M* for DMPM is marginally different only for the L31T (no. 7) and W3F,L31W (no. 9) mutants.

The rates of hydrolysis of DMPM vesicles in the scooting mode, v_o at $X_S = 1$ mole fraction in column 6 of Table 2, are in a 3-fold range. As compared in Figure 3A, the rates of hydrolysis of micellar 1,2-octanoylphosphatidylmethanol (DC_8PM) micelles are also in a comparable range with 3.5-fold higher absolute rates. Note that W3F (no. 2) has a even higher v_o with DC_8PM, which is consistent with our earlier results with the bovine PLA2 mutants where the effect is attributed to a role of the N-terminal segment in the recognition of the acyl chains in the chemical step (*41*). Apparently, Leu-31 substitution also modestly influences the chain discrimination as indicated by a significantly lower rate of hydrolysis of DMPM by the mutants with a smaller substituent (nos. 3 and 4 in Figure 3). Available evidence suggests that residues 3 and 31 are separated from each other in such a way that residues 2 and −3 contact C_8 of the *sn*-2

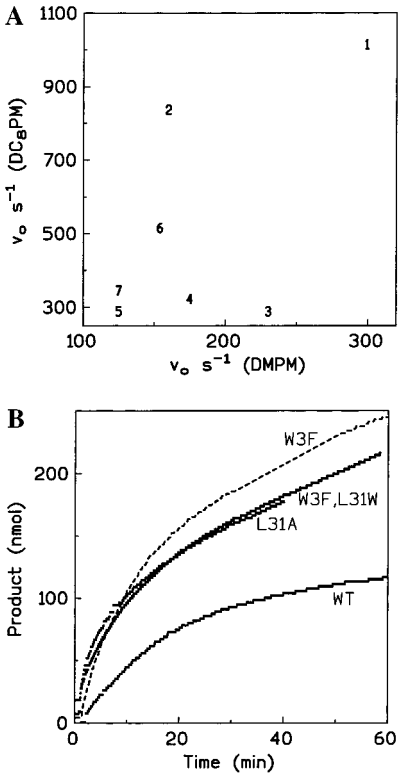

FIGURE 3: (A) Comparison of the initial rates of hydrolysis, v_o, for the hydrolysis of DC_8PM micelles (ordinate) versus DMPM vesicles by the Leu-31 substitution mutants from Table 2. (B) Reaction progress curve for the hydrolysis of 0.4 mg of DMPM vesicles (small sonicated vesicles of about 25 nm diameter) with 0.22 μg of pig pancreatic PLA2 (WT and mutants as indicated) in a 4 mL reaction mixture containing 1 mM NaCl and 0.5 mM $CaCl_2$ at 24 °C.

Table 3: Inhibition Constants [X_I(50) or Ic(50)] for WT and W3F,L31W PLA2-Catalyzed Hydrolysis of DMPM Vesicles

inhibitor[a]	WT	W3F,L31W
	X_I Values	
MG14	0.0014	0.0034
(*R*)-C14-PG	0.002	0.003
(*R*)-C14-PN	0.013	0.011
PN	0.5	0.25
deoxy-LPC	>1	0.2
MJ45	0.0023	0.003
MJ99	0.003	0.0025
	Ic(50) Values	
$KClO_4$	30 mM	130 mM
MPD	0.11 M	2 M
$KClO_3$	>0.5 M	0.26 M
propionamide	68 mM	30 mM

[a] Abbreviations: MG14, L-1-*O*-octyl-2-heptylphosphonyl-*sn*-glycero-3-phosphoethanolamine; MJ45, 1-hexadecyl-3-allyl-*rac*-glycero-2-phosphomethanol; MPD, 2-methylpentanediol; (*R*)-C14-PG, 2-(*R*)-tetradecanoylaminohexanol-1-phosphoglycerol; (*R*)-C14-PN, 2-(*R*)-tetradecanoylaminohexanol-1-phosphocholine.

chain, whereas residue 31 would be closer to C_8 of the *sn*-1 chain (*10*, *14*, *16*, *23*).

K_M* values for DMPM (column 5, Table 2) are significantly below mole fraction 1. The changes of this magnitude at $X_S = 1$ can account for less than a 2-fold change in v_o:

$$v_o = V_M^{app} = \frac{X_S k^*_{cat}}{X_S + K_M^*} \quad (2)$$

As an alternative, v_o can decrease from a perturbed binding of the mutant to DMPM vesicles (*1*, *3*, *5*). As indicated by the results in Figure 3B, at longer times after the initial processive burst of activity has virtually ceased in WT, the reaction progress curves for the three mutants are significantly different. A more rapid sustained hydrolysis at longer times seen with the three mutants can only be attributed to a slow intervesicle exchange of the enzyme (*41*, *42*). In effect, a slow E* to E desorption of the bound enzyme would modestly decrease the average turnover rate by effectively lowering the residence time of the enzyme at the interface (*5*). These effects are difficult to quantify (*42*); however, the magnitude of the observed differences v_o for DMPM is not inconsistent with a small shift in the E to E* equilibrium, yet we cannot rule out a modest effect on k^*_{cat} (also see below).

Effect on Inhibitor Binding. A modest effect of Leu-31 substitution on the binding of DMPM or deoxy-LPC implies an effect on the active site events. For example, X_I(50), the mole fraction for 50% inhibition or $v_o/v_I = 2$, is related to K_M* and K_I* as (*5*)

$$\frac{v_o}{v_I} = 1 + \left(\frac{1 + 1/K_I^*}{1 + 1/K_M^*}\right)\left(\frac{X_I}{1 - X_I}\right) \quad (3)$$

The X_I(50) values for MJ33 with DMPM vesicles (column 7, Table 2) or DC_7PC micelles (column 12, Table 2) are in a narrow range. In conjunction with the independently obtained K_M* values (column 5 in Table 2), we conclude that K_I* for MJ33 is significantly lower only for the double mutant W3F,L31W. To discern effects on the mimic binding, the X_I(50) values for several inhibitors are compared in Table 3. Note that deoxy-LPC is a somewhat better inhibitor of the double mutant, whereas PN is marginally different. The glycerophospholipid analogues with *sn*-2 phosphonate (MG14) or *sn*-2 amide (C14-PG and C14-PN) are not significantly discriminated. Since MJ45 and MJ99 (*26*) are equally potent inhibitors for WT and the double mutant, the higher affinity of the mutant for MJ33 must be attributed to the *sn*-3 substituent. In the cocrystals, the trifluoroethyl group of MJ33 makes contact with hydrophobic residues 19, 20, and 22 (*14*), and thus they could influence the calcium (26−34) loop.

A change in the active site geometry of the double mutant is also indicated by a difference in the Ic(50) values for several water-soluble inhibitors (Table 3). Tetrahedral perchlorate anion ($KClO_4$) and 2-methylpentanediol (MPD) are weaker inhibitors of the double mutant, whereas propionamide and trigonal chlorate ($KClO_3$) anion are marginally better. MPD, a commonly used additive in the crystallization solvents, is found in the active site pocket of WT PLA2. For example, of the two molecules of MPD seen in the 1.7 Å resolution structure (PDB 1BP2), one is in the substrate binding pocket at a location that is in the vicinity of the calcium loop and the carboxylate of Asp-49. A perturbed active site geometry associated with Leu-31 substitutions can also account for a small difference in the association of trigonal chlorate anion or the propionamide NH2 to δNH of His-48. The significance of the discrimination of the smaller inhibitors by WT versus the double mutant lies in the fact that their binding is likely to be dominated only by the residues close to the calcium binding site.

Hydrolysis at Zwitterionic Micelles in the Quasi-Scooting Mode. V_M^{app} for DC_8PC in Table 1 was obtained in 0.1 M NaCl, which is a significant contribution of the salt effect. Such effects are well resolved and characterized for the hydrolysis of DC_7PC at 1 mM NaCl versus 4 M NaCl (*6*). The apparent kinetic parameters obtained under the two salt conditions are analytically interpretable because during the hydrolysis of micelles of short-chain phospholipids the substrate and product exchange rapidly between micelles relative to the catalytic turnover rate. A rapid exchange ensures that the rate of substrate replenishment on the enzyme-containing micelle is rapid and that the chemical step of the turnover cycle remains rate limiting. Such local and global steady-state conditions ensure turnover in the quasi-scooting mode with virtually infinite processivity.

As summarized in Table 2, the V_M^{app} values are larger in 4 M NaCl due to the interfacial anionic charge induced by the preferential partitioning of chloride into zwitterionic micelles and vesicles. V_M^{app} (eq 2) is the rate at the bulk saturating concentration of micelles with all of the enzyme bound to the interface and $X_S = 1$. Leu-31 substitution lowers V_M^{app} by as much as 60-fold, yet the effect is modest on the apparent affinity. K_M^{app} is a complex parameter defined as (*6*)

$$K_M^{app} = \frac{K_d K_M^*}{1 + K_M^*}\left(1 + \frac{K_S'}{K_M}\right) \quad (4)$$

K_S' is the critical micelle concentration. K_M is the Michaelis constant for the monodisperse ES, which appears to be larger than K_S' on the basis of the analogue binding results (*6*). K_d is the dissociation constant for E* to E. K_M* is the Michaelis constant for the turnover at the interface. Unless several components somehow compensate for each other, we rule

Table 4: Intensity Changes in the Fluorescence Emission from W3F,L31W

treatment	state[a]	charge[a]	intensity	peak at (nm)	K_d (μM)
E	aqueous		1.0	344	
E + DTPM	b	a	−0.63	354	<2
E + DTPM + Ca	b	a	−0.17	335	<2
E + HPM	m	a	−0.50	354	20
E + HPM + Ca	m	a	−0.03	335	
E + PN	m	z	0.34	318	3200
E + Ca			−0.10	335	
E + Ca + PN	m	z	+0.20	318	74[b]
E + PC8-ether	m	z	+0.60	320	364
E + PC8-ether + NaCl	m	z	−0.20	340	
E (D_2O) + Ca	m	z	−0.026	335	
E (D_2O) + Ca + PN	m	z	+0.7	318	72[b]
E (D_2O) + DTPM	b	a	−0.55	353	<2

[a] Abbreviations: a, anionic; b, bilayer; m, micellar; z, zwitterionic. [b] These are calcium-dependent apparent constants (eq 1).

out a significant role for Leu-31 on K_d (see also Table 4). In any case, such a change cannot account for the observed effect of Leu-31 substitution on V_M^{app}.

The $X_I(50)$ values suggest that K_M* for DC_7PC is at best modestly affected by Leu-31 substitutions. The values for MJ33 are comparable for the hydrolysis of DMPM (column 7) or DC_7PC in 4 M NaCl (column 12), which suggests that K_M* values for the two substrates are marginally different for the Leu-31 substitution mutants. The possibility that both K_M* and K_I* (eq 3) could change to compensate for each other (eq 3) is discounted on the basis of the K_M^{app} values in 1 mM (column 9) or 4 M NaCl (column 11). Together, we conclude that the effect of Leu-31 substitution on K_M*, K_I*, and K_d is modest at best, and virtually all of the effect of added NaCl on K_M^{app} is attributed to a change in K_d (*6*). The origin of the salt effect lies in the preferential partitioning of chloride into the zwitterionic interface (*6*). Therefore, a large effect of Leu-31 substituion on V_M^{app} in 4 M NaCl (column 10), compared to a less than 3-fold effect seen at anionic DMPM vesicles or DC_8PM micelles, suggests a role for Leu-31 in the control of k^*_{cat} activation by the induced anionic charge at the zwitterionic interface.

Spectroscopic Properties of L31W. A significant effect of Leu-31 substitution on k^*_{cat} at the zwitterionic interface suggests that this residue somehow modulates the effect of the interfacial charge on the structure of the enzyme. Such a difference is clearly seen in the fluorescence emission properties of Trp-31 in the double mutant. For example, the Trp-31 emission spectrum of the double mutant is not influenced by the presence of calcium (Figure 4A). On the other hand, the change in the fluorescence emission spectrum, shown as the difference spectrum marked with a δ, resulting from the binding of the double mutant to anionic DTPM vesicles (Figure 4A) is qualitatively different from that obtained on the binding to micelles of zwitterionic hexadecylphosphocholine (Figure 4B). Also, at both of the interfaces the difference spectra are only modestly different in the presence of calcium. Since calcium is the obligatory cofactor for the binding of the active site directed ligand, the difference spectra in Figure 4 show that the calcium binding and the consequent occupancy of the active site have a marginal effect on the fluorescence emission from Trp-31. In contrast, the fluorescence emission changes from Trp-3 on the binding of WT PLA2 to the anionic or zwitterionic

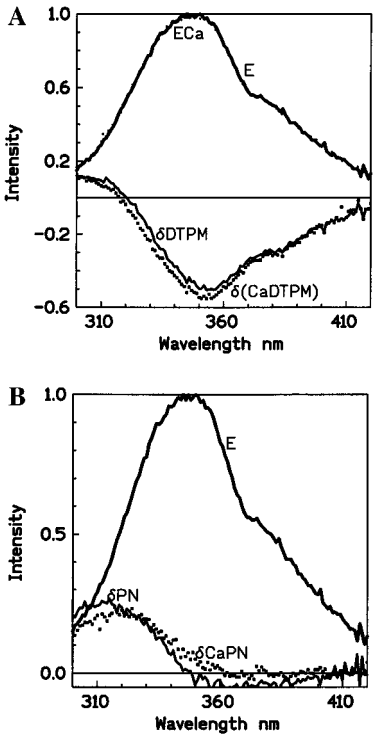

FIGURE 4: (A) Fluorescence emission spectrum of the E and E·Ca forms (top) of the W3F,L31W mutant (1 μM or 0.022 mg/1.5 mL in 10 mM Tris and 0.5 mM calcium, if present). The decrease in the emission intensity in the spectrum of the two forms on the addition of DTPM vesicles is shown as the difference spectra marked with δ. (B) Change in the fluorescence spectrum of the E and E·Ca forms of the mutant on the addition of hexadecylphosphocholine (PN) micelles. Excitation was at 280 nm with both slit widths at 4 nm. The fluorescence intensities in this and other figures are normalized to a value of 1 for the WT in the E form.

interfaces are virtually identical, and an additional increase in intensity is seen on the occupancy of the active site (*27*, *28*, *42*).

The fluorescence emission properties of Trp-31 associated with the binding of the double mutant under a variety of conditions are summarized in Table 4. Binding to DTPM vesicles decreases the emission intensity by 63% with a peak at 354 nm, compared to the peak at 344 nm for the E form of the double mutant. In contrast, the binding of the double mutant to the zwitterionic PN or PC8-ether micellar interface results in a 34% increase with a 35 nm blue shift. The interface-dependent changes in the emission intensities also depend on the bulk concentration of the amphiphile. K_d values for the E to E* equlibrium obtained from such changes are summarized in column 6 of Table 4. K_d for the double mutant at the anionic interface (DTPM bilayer or HPM micelles) is considerably smaller than it is for the zwitterionic micelles (PN and PC8-ether). Also, a lower apparent K_d at the zwitterionic interface in the presence of calcium is expected from the sequential calcium-dependent occupancy of the active site as in eq 1 (*2*).

A difference in the direction of the spectral shifts at the anionic versus zwitterionic interfaces suggests that internal quenching factors associated with local interactions may be at work. As discussed later, we attribute the difference to a direct effect of the interfacial charge on the enzyme at the interface. A possible effect of the local interactions of the glycerophosphate backbone with the i-face of PLA2 is ruled

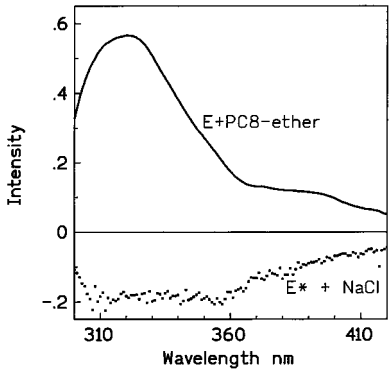

FIGURE 5: Difference emission spectra of the 1 μM W3F,L31W mutant obtained on (full line) the addition of 0.8 mM PC8-ether and (dots) the further change induced by the addition of 4 M NaCl.

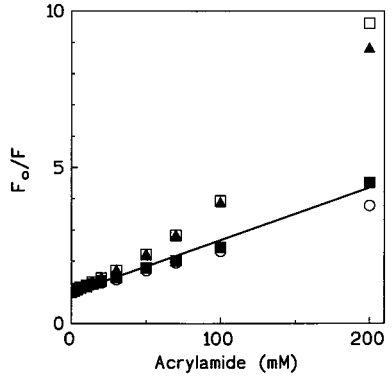

FIGURE 6: Stern−Volmer plot for the acrylamide quenching of the fluorescence emission of the W3F,L31W mutant at 345 nm in the (open square) E, (filled triangle) E·Ca, (filled square) E*·Ca·PN, and (open circle) E*·Ca·DTPM forms. The best fit line for the filled squares is also shown.

out by results in Table 4 and Figure 5. For example, the spectral change on the binding to PC8-ether micelles is analogous to that seen with PN micelles. Similarly, the difference spectra obtained with DTPM and HPM are identical. Also note that the NaCl-induced spectral change shows a trough due to a decrease in the fluorescence emission, which is analogous to the change seen on the binding to the anionic interface. Additional broadening in the 320 nm region is possibly due to the fact that the salt-induced change has an additional component from a simultaneous decrease in the fluorophore population at the zwitterionic interface.

Trp-31 in the double mutant bound to the anionic or zwitterionic interface remains accessible to acrylamide, a water-soluble quencher. As shown in the Stern−Volmer plots in Figure 6 the accessibility of Trp-31 is virtually the same in the E and E·Ca forms. An upward curvature at higher acrylamide concentrations implies a static contribution, possibly from the binding of acrylamide to the W3F,L31W mutant in the aqueous phase. In contrast, the quenching plots (Figure 6) for the E*·Ca·PN or E*·Ca·DTPM forms are linear with virtually identical slope. The acrylamide concentrations for 50% quenching are summarized in Table 5, where these values are also compared with those for the quenching of Trp-3 in WT. Typically, the acrylamide concentration for 50% quenching of Trp-3 is higher than it is for Trp-31; i.e., Trp-31 is less shielded. Moreover, the quenching concentration for Trp-3 is severalfold higher for the E*·Ca·DTPM and E*·Ca·PN forms. In comparison, the

Table 5: Acrylamide Concentration (mM) for 50% Quenching of the Fluorescence Emission from Trp-3 of WT and from Trp-31 of the W3F,L31W Mutant

form	WT[a]	W3F,L31W
E	125	42
E·Ca	130	41
E*·DTPM	700	70
E*·Ca·DTPM	750	74
E*·PN	420	55
E*·Ca·PN	550	60

[a] From refs *28* and *43*.

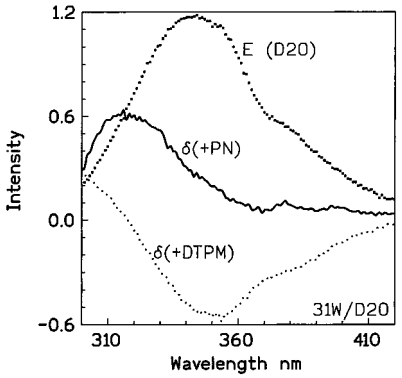

FIGURE 7: Fluorescence emission spectrum of the W3F,L31W mutant in deuterated water (D_2O) in 1 mM $CaCl_2$ and 10 mM Tris at pH 7.6 (top) normalized to the intensity of the enzyme in H_2O (=1.0 shown in Figure 3A). The difference spectra (δ) were obtained on the addition of 2 mM PN (full line) or 0.1 mM DTPM.

accessibility of Trp-31 to aqueous acrylamide changes marginally, if at all, on the binding of calcium, on the binding to the interface, or on the occupancy of the active site in the double mutant. Together, the steady-state fluorescence properties of the W3F,L31W mutant report a distinct environment of Trp-31 at the anionic versus zwitterionic interface without a significant shielding from the aqueous environment.

Accessibility of Trp-31 in the E and E* forms of the double mutant was also monitored in deuterated water. For example, the emission intensity of Trp-31 in D_2O is 18% higher (Figure 7) than it is in H_2O (Figure 4), which is attributed to quenching due to a vibrational overlap of indole and H_2O. A similar H_2O versus D_2O difference is observed for Trp-3 in WT; however, in this case no significant difference is seen in the E*·Ca·DTPM form in D_2O versus H_2O, as if Trp-3 is shielded from the aqueous environment (*27*). In contrast, Trp-31 clearly distinguishes the D_2O versus the H_2O environment of the bound form of the double mutant. For example, both in H_2O (Figure 4A) and in D_2O (Figure 7), the spectral change induced on the binding of the double mutant to DTPM is virtually identical; that is, the change is due to a component of Trp-31 emission that is not quenched by water. In contrast, the shape of the spectral change on the binding of the double mutant to PN micelles in D_2O is similar to that in H_2O; however, the emission intensity change in D_2O (Figure 6) is three times larger than it is in H_2O (Figure 4B). This difference is attributable to the interaction of Trp-31 with free or solvated water.

Together, the fluorescence results show that, irrespective of the quencher and the underlying photophysics, Trp-31 remains exposed in the bound form of the double mutant.

The difference spectra show a difference in the microenvironment at the anionic versus zwitterionic interfaces. In PN micelles, but not in DTPM, Trp-31 is significantly quenched by solvation or interactions involving protonation or hydrogen bonding. On the basis of the kinetic and fluorescence properties of Trp-31, we conclude that PLA2 at the two interfaces is present in two structurally distinct forms.

DISCUSSION

The evidence for the two forms of the pig pancreatic PLA2 at the zwitterionic versus anionic interfaces is a significant result. It provides a structural basis for the k^*_{cat} activation by the interfacial anionic charge, as induced by the bile salts in the physiological environment of the pancreatic PLA2. The observed rates at the anionic interface are higher by 2−6 orders of magnitudes under a variety of conditions (*4*, *21*). The overall effect can be attributed to two parameters. Up to a 100-fold decrease in K_d is seen at the anionic interface, which accounts for much of the rate enhancement seen under most assay conditions where the substrate concentration is typically in the submillimolar range. In addition, the anionic charge at the interface also increases the interfacial turnover rate through a direct effect on k^*_{cat} for the chemical step (6).

The structural basis for the possibly allosteric origin of k^*_{cat} activation of pancreatic PLA2 by the interfacial anionic charge remains to be established. Elsewhere we have shown that certain lysine to methionine substitutions increase k^*_{cat} at the zwitterionic interface without an effect on the rate at the anionic interface (*9*). On the basis of the premise of the k^*_{cat} activating effect of the charge neutralization of lysine-53, -56, -120, and -121 in the bound form of PLA2 (*6*), we have suggested that the bound form of PLA2 could exist in two functionally different forms at the anionic versus zwitterionic interfaces, E_a* and E_z* forms, respectively (*9*). This is now supported by the analysis of the Leu-31 substitution mutants, where the kinetic and spectroscopic results show that Trp-31 senses two different environments at the zwitterionic versus anionic interfaces. Note that the results are consistent with the k^*_{cat} activation mechanism in which both of the forms at the interface bind the substrate and mimics but differ in the chemical step. Since a modest difference is apparent in the binding of certain mimics, we attribute the k^*_{cat} activation to an interface-dependent change in the geometry of the catalytic site of the E_a*·Ca·S and E_z*·Ca·S complexes that undergo the chemical change with only a modest difference in the K_M* values. While the properties of the two forms adequately account for the kinetic behavior, the challenge of the structural characterization of the forms of PLA2 at the interface lies ahead.

Insights into the i-Face. While the structural details of the bound form(s) of pancreatic PLA2 at the interface remain to be worked out, as a prelude to the future work we continue to develop key arguments in the context of the crystal structure of PLA2. Operationally, the molecular contact of PLA2 with the interface occurs along the i-face, which we have proposed to be on the bottom plane for the orientation in Figure 8. In this figure the idealized plane of the i-face would be perpendicular to the plane of the paper (*23*). Trp-3 in WT is a part of the i-face shielded from the aqueous phase in the E* and E*·L forms (*23*, *27*, *28*, *41*, *42*). However, contrary to earlier suggestions (*16*, *22*, *25*, *32*, *38*), the criteria and protocols in the present study show that Leu-31 is not a part of the i-face. In Figure 8 this is emphasized by the fact that Trp-3 is at the bottom surface in contact with the interface, whereas residue 31 is near the bottom edge on the front surface exposed to the aqueous environment. A hydrophobic contact of residue 31 with the interface is also inconsistent with the fact that out of the 53 PLA2 sequences (*44*) Leu-31 is found in only the pancreatic PLA2 (8 sequences), and some of the PLA2 sequences contain arginine (11 cases) and lysine (3). Leu-31 is also found in the newly discovered classes of mammalian secreted PLA2 (types IIA−E, V, and X) along with the cationic residues in positions 53 and 56 and near the C-terminus (*45*). It would be instructive to find out how the anionic interface preference of these enzymes correlates with the distribution of the cationic residues in the vicinity of the i-face. Also note that some of the snake venom PLA2 sequences, for example, type IA with cationic residue 31 and neutral or anionic residues 53, 56, and 120, do not show a preference for the interfacial anionic charge.

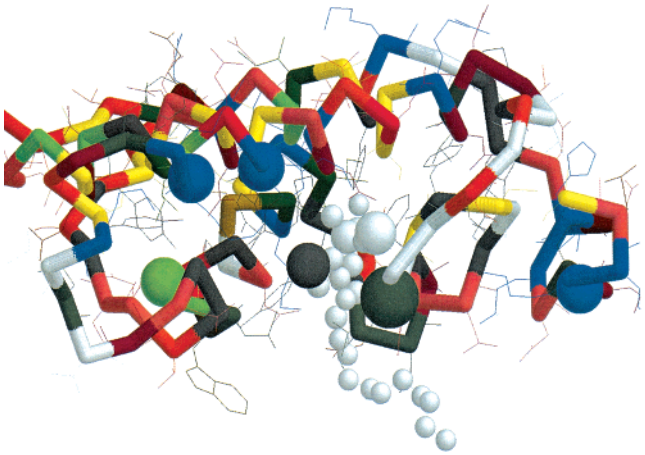

FIGURE 8: Suggestive orientation of pancreatic PLA2 [PDB 1FDK (*14*)] at the interface (not shown). The i-face (the bottom face in this orientation) of PLA2 aligns along with Leu-2, Trp-3, Leu-19, Met-20, and Phe-22, which make contact with the interface (*23*). Thus the plane along the i-face and perpendicular to the plane of the paper would be the substrate interface. A slot in the i-face is well suited for binding of the substrate from the interface to the active site. The structure with gray balls is MJ33 in the active site of the crystal structure. In this visualization the hexadecyl chain of the inhibitor extends into the interface along the i-face. Leu-31 (right) and Tyr-69 (left) are marked as black balls near the lower edge of the front face. The orientation and alignment of these residues relative to the interface are influenced by the neutralization of the cationic residues 53, 56, and 120 (blue balls). The green ball is the amino group of Ala-1. Such changes could facilitate removal of the product from the slot in the front face.

How does Trp-31 in the double mutant experience different environments at the anionic versus zwitterionic interfaces? We surmise that Leu-31 mediates the k^*_{cat} activation through a yet uncharacterized specific contact with the anionic interface. Elsewhere we have developed evidence that cationic residues 53, 56, 120, and 121 of pancreatic PLA2 mediate the preference for the interfacial anionic charge (*9*, *11*, *13*). These cationic residues are on the front face (Figure 8), however somewhat removed from the bottom edge of the i-face. Therefore, charge neutralization of the cationic residues by the anionic interface could realign E_z*·Ca·S into a catalytically more efficient E_a*·Ca·S form. Thus the

hydrophobic side chain of Leu-31 could play a significant role in aligning the E_a*•S form at the anionic interface. As a part of the calcium loop, Leu-31 is in a position to control the chemical step (*12*). Also, in the consensus catalytic mechanism (*12*, *16*, *20*, *21*), the carbonyl oxygen of the substrate is believed to H-bond to the backbone NH of Gly-30 and the interaction persists with the tetrahedral mimics (*14*). Thus interactions of Leu-31 could play a role in stabilizing the tetrahedral intermediate.

There are other features of interest in the control of the calcium loop by the interface and by the charge at the interface. As shown in Figure 8, Leu-31 and Tyr-69 are on the same face of the PLA2. Both, Leu-31 and Tyr-69, are not conserved residues. For example, in the 53 sequences compared by Van den Bergh et al. (*44*), Tyr-69 (22 cases) is replaced by lysine (29 cases) and serine. Similarly, in these 53 sequences, Leu-31 is found only in the pancreatic PLA2 sequences (8 cases). In all other cases residue 31 is arginine (11 cases), lysine (3), tryptophan (13), alanine (11), or proline, valine, or serine. Although a hydrophobic or charged residue is not critical in positions 31 or 69, or both, in none of the 53 sequences is a charged residue found in both of these positions.

Both Tyr-69 and Leu-31 are separated by a cleft to the active site pocket. This cleft is somewhat narrower than the bottom slot on the i-face through which the acyl chain of MJ33 putatively extends into the interface (Figure 8). Recall that the Y69F mutant is k^*_{cat} impaired at the zwitterionic and anionic interfaces (*12*). This effect was interpreted in terms of a role for the hydroxyl group of Tyr-69 hydrogen bonded to the *sn*-3 phosphate of the substrate in the rate-limiting chemical step. Such a contact is seen in the structure of the cocrystals of PLA2 with substrate mimics (*15*, *16*). In the absence of a mimic in the active site, the tyrosyl side chain appears to swing out in the aqueous phase. Since Leu-31 and Tyr-69 substitutions do not significantly change the stability of the Michaelis complex, an effect on k^*_{cat} implies that these two residues somehow control the chemical step. Note that the cleft on the front face in Figure 8 is covered by the side chains of Tyr-69 and Leu-31. This arrangement raises the possibility that the cleft could facilitate removal of the product from the active site. Since the substrate enters the active site from the slot on the i-face, a physical separation of the substrate binding and the product dissociation steeps could effectively increase the turnover rate.

To recapitulate a continuing (*13*, *23*) quest for a consistent structural basis for the interfacial catalysis and activation, on the basis of the results in this paper we surmise that a hydrophobic residue in position 31 or 69 aligns the active site of pancreatic PLA2 during the catalytic turnover at the anionic interface. In this orientation of the i-face of pancreatic PLA2 (*23*), Lys-53 and -56 are on one side (*9*) and Lys-120 and -121 (*11*) on the other side of the calcium binding (26−32) loop. Neutralization of these cationic residues at the anionic interface could change the alignment of the calcium loop relative to the interface. In this orientation residues 31 and 69 are reasonably far away from the interface to ensure a hydrophobic contact, yet they influence the events of the chemical step (*12*). Changes in the alignment of residue 31 could control not only the effective oxyanionin hole by the hydrogen bonding to NH of Gly-30 (*16*, *20*, *21*) but also the catalytic water coordinated to the catalytic cofactor which makes the decomposition of the tetrahedral intermediate rate limiting (*12*, *46*). In addition, changes in the side chains of Tyr-69 and Leu-31 could facilitate the dissociation of the products from the active site through a cleft that is structurally different from the active site slot on the i-face through which the substrate binding is postulated to occur.

REFERENCES

1. Jain, M. K., Rogers, J., Jahagirdar, D. V., Marecek, J. F., and Ramirez, F. (1986) *Biochim. Biophys. Acta 860*, 435−447.
2. Jain, M. K., Yu, B.-Z., and Berg, O. G. (1993) *Biochemistry 32*, 11319−11329.
3. Jain, M. K., Gelb, M. H., Rogers, J., and Berg, O. G. (1995) *Methods Enzymol. 249*, 567−614.
4. Jain, M. K., and Berg, O. G. (1989) *Biochim. Biophys. Acta 1002*, 127−156.
5. Berg, O. G., Yu, B.-Z., Rogers, J., and Jain, M. K. (1991) *Biochemistry 30*, 7283−7297.
6. Berg, O. G., Rogers, J., Yu, B., Yao, J., Romsted, L. S., and Jain, M. K. (1997) *Biochemistry 36*, 14512−14530.
7. Berg, O. G., Cajal, Y., Butterfoss, R. L., Grey, R. L., Alsina, M. A., Yu, B. Z., and Jain, M. K. (1998) *Biochemistry 37*, 6615−6627.
8. Jain, M. K., Rogers, J., Gelb, M. G., Tsai, M.-D., Hendrickson, E. K., and Hendrickson, S. (1992) *Biochemistry 31*, 7841−7847.
9. Rogers, J., Yu, B. Z., Tsai, M. D., Berg, O. G., and Jain, M. K. (1998) *Biochemistry 37*, 9549−9556.
10. Liu, X., Zhu, H., Huang, B., Rogers, J., Yu, B. Z., Kumar, A., Jain, M. K., Sundaralingam, M., and Tsai, M. D. (1995) *Biochemistry 34*, 7322−7334.
11. Huang, B., Yu, B. Z., Rogers, J., Byeon, I. L., Sekar, K., Chen, X., Sundaralingam, M., Tsai, M. D., and Jain, M. K. (1996) *Biochemistry 35*, 12164−12174.
12. Yu, B. Z., Rogers, J., Nicol, G., Theopold, K. H., Seshadri, K., Vishweshwara, S., and Jain, M. K. (1998) *Biochemistry 37*, 12576−12587.
13. Yu, B. Z., Rogers, J., Tsai, M. D., Pidgeon, C., and Jain, M. K. (1999) *Biochemistry 38*, 4875−4884.
14. Sekar, K., Eswaramoorthy, S., Jain, M. K., and Sundaralingam, M. (1997) *Biochemistry 36*, 14186−14191.
15. Thunnissen, M. M. G. M., Ab, E., Kalk, K. H., Drenth, J., Dijkstra, B. W., Kuipers, O. P., Dijkman, R., de Haas, G. H., and Verheij, H. M. (1990) *Nature 347*, 689−691.
16. Scott, D., and Sigler, P. (1994) *Adv. Protein Chem. 45*, 53−88.
17. Yuan, C., Li, Y., Byeon, I., Poi, M., and Tsai, M. D. (1999) *Biochemistry 38*, 2919−2929.
18. Van den Berg, B., Tessari, M., de Haas, G. H., Verheij, H. M., Boelens, R., and Kaptein, R. (1995) *EMBO J. 14*, 4123−4131.
19. Van den Berg, B., Tessari, M., Boelens, R., Dijkman, R., Kaptein, R., de Haas, G. H., and Verheij, H. M. (1995) *J. Biomol. NMR 5*, 110−121.
20. Verheij, H. M., Volwerk, J. J., Jansen, E. H. J. M., Puijk, W. C., Dijkstra, B. W., Drenth, J., and de Haas, G. H. (1980) *Biochemistry 19*, 743−740.
21. Verheij, H. M., Slotboom, A. J., and de Haas, G. H. (1981) *Rev. Physiol. Biochem. Pharmacol. 91*, 91−203.
22. Dijkstra, B. W., Drenth, J., and Kalk, K. H. (1981) *Nature 289*, 604−606.
23. Ramirez, F., and Jain, M. K. (1991) *Proteins: Struct., Funct., Genet. 9*, 229−239.
24. Kuipers, O. P., Kerver, J., van Meersbergen, J., Vis, R., Dijkman, R., Verheij, H. M., and de Haas, G. H. (1990) *Protein Eng. 3*, 599−603.
25. Kuipers, O. P., Vincent, M., Brochon, J. C., Verheij, H. M., de Haas, G. H., and Gallay, J. (1991) *Biochemistry 30*, 8771−8785.
26. Jain, M. K., Tao, W., Rogers, J., Arenson, C., Eibl, H., and Yu, B.-Z. (1991) *Biochemistry 30*, 10256−10268.

27. Jain, M. K., and Vaz, V. L. C. (1987) *Biochim. Biophys. Acta 905*, 1−8.
28. Maliwal, B. P., Yu, B. Z., Szacinski, H., Squier, T., Van Binsbergen, J., Slotboom, A. J., and Jain, M. K. (1994) *Biochemistry 33*, 4509−4516.
29. Lugtigheid, R. B., Otten-Kuipers, M. A., Verheij, H. M., and de Haas, G. H. (1993) *Eur. J. Biochem. 213*, 517−522.
30. Lugtigheid, R. B., Nicolaes, G. A. F., Veldhuizen, E. J. A., Slotboom, A. J., Verheij, H. M., and de Haas, G. H. (1993) *Eur. J. Biochem. 216*, 519−525.
31. van den Bergh, C. J. A., Bekkers, A. P. A., Verheij, H. M., and de Haas, G. H. (1989) *Eur. J. Biochem. 182*, 307−313.
32. Kuipers, O. P., Dekker, N., Verheij, H. M., and de Haas, G. H. (1990) *Biochemistry 29*, 6094−6102.
33. Janssen M. J. W., Burghout, P., Verheij, H. M., Slotboom A. J., and Egmond, M. R. (1999) *Eur. J. Biochem. 263*, 782−788.
34. Kuipers, O. P., Thunnissen, M. G. M. M., De Geus, P., Dijkstra, B. W., Drenth, J., Verheij, H. M., and de Haas, G. H. (1989) *Science 244*, 82−85.
35. Beiboer, S. H. W., Franken, P. A., Cox, R. C., and Verheij, H. M. (1995) *Eur. J. Biochem. 231*, 747−753.
36. Franken, P. A., Van den Berg, L., Huang, J., Gunyuzlu, P., Lugtigheid, R. B., Verheij, H. M., and de Haas, G. H. (1992) *Eur. J. Biochem. 203*, 89−98.
37. Lugtigheid, R. B. (1993) Ph.D. Thesis, Utrecht University.
38. Han, S. K., Kim, K. P., Koduri, R., Bittova, L., Monoz, N. M., Leff, A. R., Wilton, D. C., Gelb, M. H., and Cho, W. (1999) *J. Biol. Chem. 274*, 11881−11888.
39. Yu, B. Z., Berg, O. G., and Jain, M. K. (1999) *Biochemistry 38*, 10449−10456.
40. Yu, B. Z., Berg, O. G., and Jain, M. K. (1993) *Biochemistry 32*, 6485−6492.
41. Liu, X., Xhu, H., Huang, B., Rogers, J., Yu, B., Kumar, A., Jain, M. K., Sundaralingam, M., and Tsai, M. D. (1995) *Biochemistry 34*, 7322−7334.
42. Jain, M. K., Rogers, J., Berg, O. G., and Gelb, M. H. (1991) *Biochemistry 30*, 7340−7348.
43. Jain, M. K., and Maliwal, B. P. (1993) *Biochemistry 32*, 11838−11846.
44. Van den Bergh, C. J., Slotboom, A. J., Verheij, H. M., and de Haas, G. H. (1989*) J. Cell. Biochem. 39*, 379−390.
45. Valentin, E., Ghomaschci, F., Gelb, M. H., Luzdunski, M., and Lambeau, G. (1999) *J. Biol. Chem. 274*, 31195−31202.
46. Schurer, G., Lanig, H., and Clark, T. (2000) *J. Phys. Chem. B 104*, 1349−1361.

BI9925470